Design and characterization of sulfamethoxazole derivatives as potent corrosion inhibitors: insights from polarization studies

S.S.M. AL-Gubouri and S.F. Narren*

Department of Chemistry, College of Science for women, University of Baghdad, 10001, Baghdad, Iraq
**E-mail: Shethafn_chem@csw.uobaaghdad.edu.iq*

Abstract

In this study, we present the synthesis and detailed characterization of novel sulfamethoxazole derivatives, designed to investigate their efficacy as corrosion inhibitors for mild steel in acidic environments. The synthesized compounds were analyzed using a range of spectroscopic techniques, including FTIR and ^{1}H-NMR, to confirm their chemical structures and assess their purity. Electrochemical methods, particularly potentiodynamic polarization, were employed to evaluate the corrosion inhibition properties of these derivatives in a 1 M HCl solution. The results demonstrated that the sulfamethoxazole derivatives exhibit significant inhibition efficiencies, with values reaching up to 96%, depending on the concentration and experimental conditions. The potentiodynamic polarization studies revealed that the inhibitors function by forming a stable and protective adsorption layer on the metal surface, effectively reducing the corrosion rate. Additionally, the adsorption behavior was influenced by the structural features of the derivatives, including the presence of heteroatoms that enhance their affinity for metal surfaces. The findings suggest that these novel sulfamethoxazole derivatives are promising candidates as corrosion inhibitors, demonstrating strong potential for practical application in industrial settings where metal protection in corrosive environments, such as acidic conditions, is critical.

Received: September 2, 2024 Published: October 23, 2024 doi: 10.17675/2305-6894-2024-13-4-11

Keywords: *sulfamethoxazole derivatives, corrosion inhibition, polarization technique, mild steel, adsorption mechanism.*

1. Introduction

Corrosion is a significant problem affecting various industries such as oil and gas, automotive, construction, and marine sectors, resulting in economic losses and potential safety risks. Metal degradation, especially in harsh environments like acidic conditions, calls for effective corrosion inhibitors to extend the life of metallic structures and reduce maintenance costs. Among the numerous strategies to combat corrosion, organic compounds have gained attention due to their ability to form protective layers on metal surfaces, thereby preventing interaction with corrosive species [1–5]. Heterocyclic compounds, which contain heteroatoms like nitrogen, oxygen, sulfur, or phosphorus in their ring structures, have been extensively studied for their corrosion inhibition properties. The structural diversity of these

compounds, influenced by the heteroatom's nature and position, allows for the design of molecules tailored for specific applications. Heterocyclic compounds are indispensable in corrosion science because of their ability to adsorb onto metal surfaces and form stable, protective layers [6–9]. These layers block corrosive agents like chloride ions, oxygen, and moisture from reaching the metal surface, thus inhibiting the corrosion process [10–13].

Studies have shown the effectiveness of heterocyclic compounds in protecting metals like steel, copper, and aluminum in various corrosive environments. For example, oxazoles and triazoles, particularly benzotriazoles, are known to inhibit the corrosion of steel, aluminum, and copper alloys by forming stable adsorption layers on the metal surface [14–17]. The electron-rich heterocyclic rings facilitate strong adsorption onto metal surfaces, with the electronic properties and functional groups of the compounds playing a critical role in the stability of these adsorption interactions. The presence of electron-donating groups can increase electron density on the heterocycle, enhancing metal interaction and corrosion inhibition efficiency. Sulfamethoxazole, an antibacterial agent in the sulfonamide class, has been used to treat bacterial infections, and its chemical structure features a sulfonamide group attached to a heterocyclic ring. Given its success as a therapeutic agent, sulfamethoxazole and its derivatives have been explored for non-medical applications, including corrosion inhibition. The sulfonamide group and heterocyclic ring are expected to contribute to the strong adsorption of sulfamethoxazole derivatives onto metal surfaces, forming a protective layer that shields the metal from corrosive agents, thus reducing corrosion [18]. The electron-donating properties of the sulfonamide group enhance interaction with metal surfaces, contributing to the corrosion inhibition performance [19]. The corrosion inhibition process typically involves adsorption of inhibitor molecules onto the metal surface, followed by the formation of a protective film that acts as a barrier between the metal and the corrosive environment. In sulfamethoxazole derivatives, the sulfonamide group plays a critical role by increasing electron density on the heterocyclic ring, facilitating strong adsorption onto the metal surface. This strong adsorption leads to the formation of a stable protective film that hinders the diffusion of corrosive agents like chloride ions and oxygen [20, 21]. The thickness, strength, and homogeneity of the protective film are crucial factors influencing its effectiveness, especially in highly corrosive environments [22, 23]. The development of novel corrosion inhibitors based on sulfamethoxazole derivatives offers a promising, eco-friendly approach to mitigating metal corrosion. By leveraging the structural and electronic properties of sulfamethoxazole, this research aims to contribute to the advancement of corrosion science and the design of effective organic inhibitors. This study focuses on synthesizing and characterizing sulfamethoxazole derivatives (**S1** and **S2**) (Figure 1) and evaluating their efficacy as corrosion inhibitors for mild steel in acidic environments. Using electrochemical techniques, including polarization studies, and spectroscopic methods, the research seeks to elucidate the adsorption mechanisms of these compounds on metal surfaces and the structural factors influencing their inhibition efficiency.

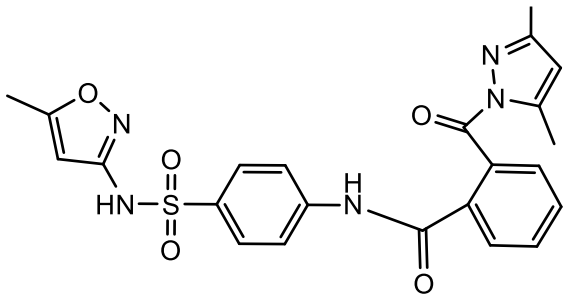

S1

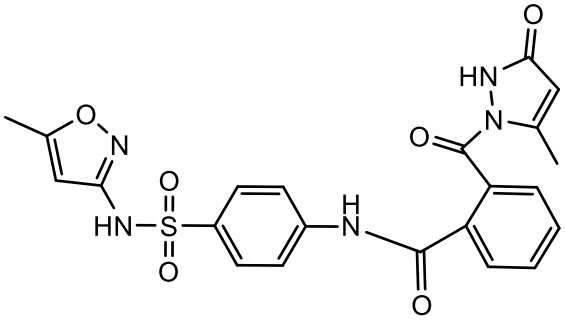

S2

Figure 1. The chemical structure of **S1** and **S2**.

2. Materials and Methods

2.1. Chemicals

All chemicals used in this study were of the highest available purity and were employed without further purification. The key chemicals utilized include absolute ethanol (99.9% purity, supplied by GCC), acetyl acetone (99% purity, provided by ISOTECINC), acetone (97% purity, from BDH), carbon disulfide (99% purity, obtained from Thomas Baker), chloroform (99.8% purity, sourced from ISOTECINC), diethyl ether (98% purity, provided by BDH), and dimethyl sulfoxide (DMSO) (99% purity, supplied by Sigma-Aldrich). Additionally, ethyl acetoacetate (99% purity, from ISOTECINC), hydrochloric acid (80% purity, from BDH), hydrazine hydrate (99% purity, supplied by GCC), maleic anhydride (99% purity, from BDH), phthalic anhydride (99% purity, provided by Merck), sulfamethoxazole (99.8% purity, obtained from Samarra), succinic anhydride (99% purity, from BDH), sodium hydroxide (99% purity, from Thomas Baker), sulfuric acid (99% purity, provided by GCC), thiosemicarbazide (99% purity, supplied by GCC), and 4-hydroxybenzaldehyde (99% purity, from BDH) were essential for the synthesis and characterization processes in this research.

*Synthesis of 2-((4-(N-(5-methylisoxazol-3-yl)sulfamoyl)phenyl)carbamoyl)benzoic acid (compound **1**)*

The synthesis began with the dissolution of 5 g (0.02 mol) of sulfamethoxazole in 15 mL of acetone. This solution was added dropwise to a solution of 0.02 mol of phthalic anhydride, also dissolved in 15 mL of acetone, with continuous stirring at room temperature for 3–4 hours. The completion of the reaction was monitored using Thin Layer Chromatography (TLC). The resulting amic acid was then filtered, washed with diethyl ether, dried, and purified using absolute ethanol. The product, a brown compound identified as 2-((4-(*N*-(5-methylisoxazol-3-yl)sulfamoyl)phenyl)carbamoyl)benzoic acid, was obtained with a yield of 88% and a melting point of 255–257°C [24].

*Synthesis of ethyl 2-((4-(N-(5-methylisoxazol-3-yl)sulfamoyl)phenyl)carbamoyl) benzoate (compound **2**)*

A mixture of 0.001 mol of the synthesized compound **1** and 5 mL of absolute ethanol with 6–8 drops of concentrated H_2SO_4 was refluxed for 5–6 hours. The progress of the reaction was monitored by TLC. Upon completion, the reaction mixture was poured into distilled water to precipitate the product, which was then filtered and purified using absolute ethanol. The final product, a pale brown compound **2**, was obtained with a yield of 68% and a melting point of 180–182°C [25].

*Synthesis of 2-(hydrazinecarbonyl)-N-(4-(N-(5-methylisoxazol-3-yl)sulfamoyl)phenyl)-benzamide (compound **3**)*

For this synthesis, a mixture of 0.001 mol of the previously synthesized compound **2** and 0.001 mol of hydrazine hydrate (99%) in 5 mL of absolute ethanol was refluxed for 6–7 hours. The reaction completion was confirmed by TLC. The mixture was then cooled, filtered, and the product purified using absolute ethanol. The resultant light brown compound, compound **3**, was obtained with a yield of 80% and a melting point of 167–169°C.

*Synthesis of corrosion inhibitors (**S1**) and (**S2**)*

To synthesize the corrosion inhibitors, a mixture of 0.001 mol of compound **3** and 0.001 mol of either acetylacetone or ethyl acetoacetate was dissolved in 5 mL of absolute ethanol. This mixture was then refluxed for 7–8 hours. Upon completion, as confirmed by TLC, the reaction mixture was cooled, filtered, and the products were purified using an ethanol/H_2O (1:1) solution. The dark brown compound (**S1**), identified as 2-(3,5-dimethyl-1*H*-pyrazole-1-carbonyl)-*N*-(4-(*N*-(5-methylisoxazol-3-yl)sulfamoyl)phenyl)benzamide, and the violet compound (**S2**), identified as 2-(5-methyl-3-oxo-2,3-dihydro-1*H*-pyrazole-1-carbonyl)-*N*-(4-(*N*-(5-methylisoxazol-3-yl)sulfamoyl)phenyl)benzamide, were obtained with yields of 92% and 80% and melting points of 125–127°C and 190–192°C, respectively.

2.2. Corrosion measurements

Preparation of specimens

The carbon steel specimens used in this study had the following composition: 0.36–0.42% C, 0.15–0.30% Si, 1.00–1.40% Mn, 0.05% P, 0.05% S, 0.50% Cu, 0.20% Ni, 0.20% Cr, and 96.88–97.49% Fe. The specimens were 1 cm in diameter and were used for polarization studies. The samples were polished sequentially using a belt grinding machine and a series of different grit emery papers (80, 150, 220, 240, 320, 400, 1000, 1200, and 2000). A solution containing 5 mg of the synthesized corrosion inhibitors (**S1**) and (**S2**) dissolved in 100 mL of DMSO was prepared. The carbon steel plates were immersed in this solution and subjected to a 1 M HCl acidic medium to evaluate the corrosion inhibition efficacy of the synthesized inhibitors [26].

Potentiostatic polarization study

The potentiostatic setup used in this study comprised a host computer, a thermostat, a magnetic stirrer, and a potentiostat/galvanostat (EmStat 4s, Palm Sens, Holland). The electrochemical corrosion cell consisted of a Pyrex cell with a 250 mL capacity, featuring both interior and exterior bowls. The cell was equipped with three electrodes: a carbon steel working electrode, a platinum auxiliary electrode (10 cm in length), and a saturated calomel electrode (Hg/Hg_2Cl_2 sat. KCl) serving as the reference electrode [27, 28]. After immersing the working electrode in the test solution for 15 minutes to establish the steady-state open circuit potential (E_{ocp}), electrochemical measurements were conducted over a potential range of ±200 mV. All tests were performed at 298 K using a cooling-heating circulating water bath. The corrosion potential (E_{corr}) and corrosion current density (i_{corr}) were determined by extrapolating the anodic and cathodic Tafel slopes in the presence and absence of the inhibitor molecules in a 1 M HCl solution.

The inhibition efficiency (%*IE*) was calculated using the following Equation:

$$IE\% = \frac{i_{corr}^{0} - i_{corr}}{i_{corr}} \cdot 100$$

where i_{corr}^{0} is the corrosion current density in the absence of inhibitors, and i_{corr} is the corrosion current density in the presence of inhibitors. This Equation was employed to evaluate the effectiveness of the synthesized sulfamethoxazole derivatives as corrosion inhibitors.

Polarization resistance is calculated by the inverse of the slope of the current density *vs.* potential curve near the corrosion potential (E_{corr}). The Equation is:

$$R_p = \frac{B}{i_{corr}}$$

- R_p is the polarization resistance ($\Omega \cdot cm^2$)
- B is the Tafel constant, which depends on the anodic (β_a) and cathodic (β_c) Tafel slopes.
- i_{corr} is the corrosion current density (A/cm^2).

The value of B can be derived as:

$$B = \frac{\beta_a \cdot \beta_c}{2.303\left(\beta_a + \beta_c\right)}$$

- β_a is the anodic Tafel slope (V/decade).
- β_c is the cathodic Tafel slope (V/decade).

The corrosion rate in mm/year (millimeters per year) can be calculated using the following Equation:

$$C_R = \frac{K \cdot i_{corr} \cdot EW}{\rho}$$

- C_R is the corrosion rate (mm/year).
- K is a constant that depends on the units used (for current density in μA/cm^2, K = 3272).
- i_{corr} is the corrosion current density (A/cm² or μA/cm^2).
- EW is the equivalent weight of the metal (g/equivalent).
- ρ is the density of the metal (g/cm^3).

3. Results and Discussion

3.1. Chemistry

Schematic Figure 2 illustrates the multi-step synthetic route used to develop novel sulfamethoxazole derivatives and their subsequent conversion into corrosion inhibitors (**S1**) and (**S2**). The synthetic pathway begins with the reaction of sulfamethoxazole with phthalic anhydride, forming the intermediate 2-((4-(*N*-(5-methylisoxazol-3-yl)sulfamoyl) phenyl)carbamoyl)benzoic acid (compound **1**). This step involves a nucleophilic acyl substitution reaction where the amino group of sulfamethoxazole reacts with the anhydride group of phthalic anhydride, leading to the formation of an amic acid derivative. In the next step, compound **1** is esterified using ethanol and sulfuric acid as a catalyst, yielding ethyl 2-((4-(*N*-(5-methylisoxazol-3-yl)sulfamoyl)phenyl)carbamoyl) benzoate (compound **2**). The esterification reaction involves the conversion of the carboxylic acid group into an ester, a common modification that often increases the lipophilicity of the molecule, which could influence its adsorption behavior on metal surfaces in corrosion inhibition applications. The third step involves the hydrazinolysis of compound **2** with hydrazine hydrate, resulting in the formation of the hydrazide derivative, 2-(hydrazinecarbonyl)-*N*-(4-(*N*-(5-methylisoxazol-3-yl)sulfamoyl)phenyl)benzamide (compound **3**). Hydrazinolysis replaces the ester group with a hydrazide group, introducing an additional nucleophilic center into the molecule. This modification is particularly relevant for corrosion inhibition, as hydrazides can enhance the compound's ability to form stable complexes with metal ions. The final step in the synthetic sequence involves the cyclization of compound **3** with either acetylacetone or ethyl acetoacetate. The reaction of compound **3** with acetylacetone yields the pyrazole-based corrosion inhibitor (**S1**), 2-(3,5-dimethyl-1*H*-pyrazole-1-carbonyl)-*N*-(4-(*N*-(5-methylisoxazol-3-yl)sulfamoyl)phenyl) benzamide. Similarly, the reaction with ethyl acetoacetate leads to the formation of the pyrazolone-based inhibitor (**S2**), 2-(5-methyl-3-oxo-2,3-dihydro-1*H*-pyrazole-1-carbonyl)-*N*-(4-(*N*-(5-methylisoxazol-3-yl)sulfamoyl)phenyl)-benzamide. Both these reactions are typical examples of condensation reactions, where the hydrazide reacts with a β-diketone to form a five-membered pyrazole or pyrazolone ring. These final products, (**S1**) and (**S2**), represent new classes of corrosion inhibitors containing

the pyrazole and pyrazolone moieties, respectively. The presence of the pyrazole ring is particularly significant, as pyrazoles are known for their strong coordination ability with metal surfaces, thereby enhancing their potential as effective corrosion inhibitors. The introduction of these heterocyclic rings into the sulfamethoxazole backbone not only potentially enhances the electronic properties of the molecule but also facilitates better adsorption on metal surfaces due to the increased availability of lone pair electrons and π-electrons, which can interact with the metal.

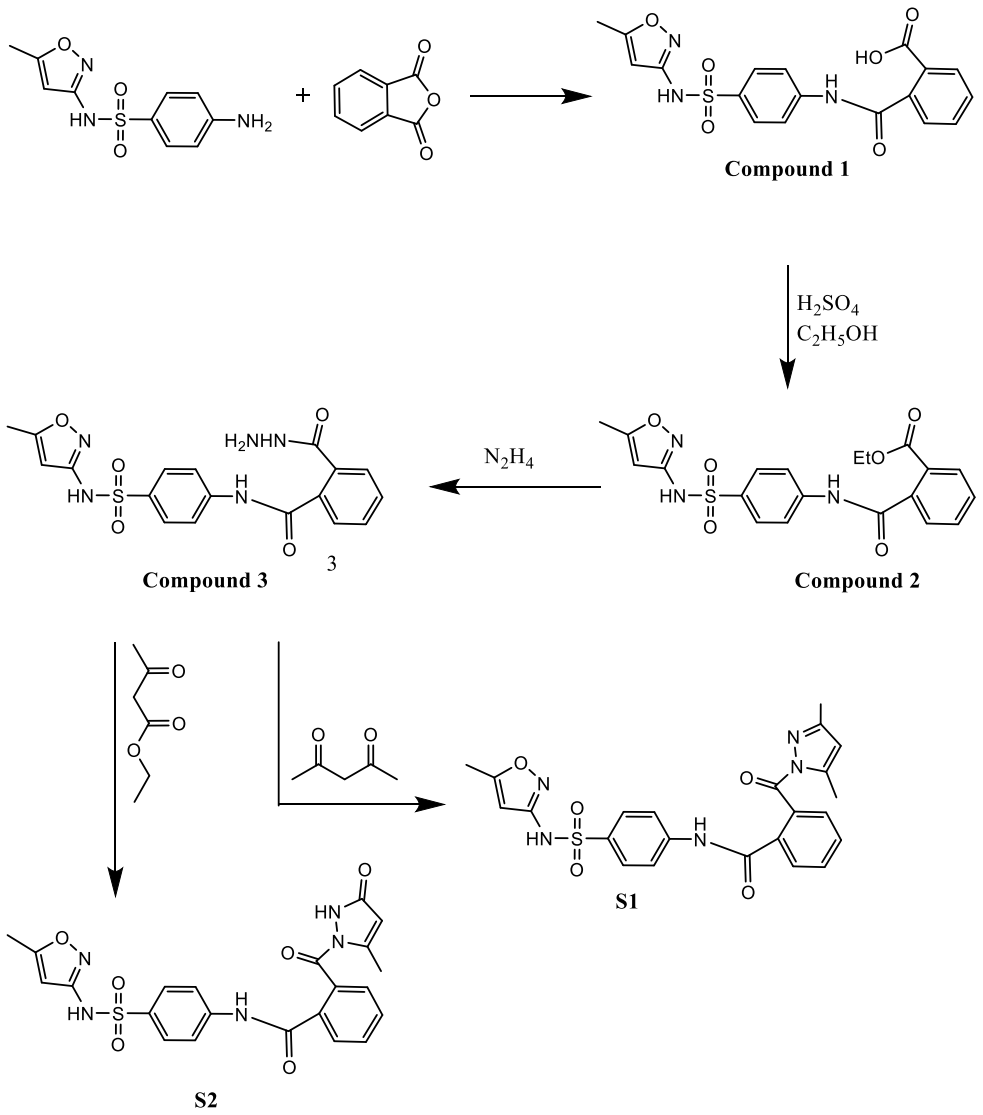

Figure 2. Synthesis of sulfamethoxazole derivatives and their conversion to corrosion inhibitors **S1** and **S2**.

The compound **1** was synthesized through the reaction of sulfamethoxazole with phthalic anhydride in the presence of acetone as a solvent, conducted in an ice bath. This reaction leads to the formation of an amic compound via the nucleophilic attack of the amino group in the sulfamethoxazole on the carbonyl group of the phthalic anhydride. This

synthetic approach is typical in organic chemistry for forming amide linkages, which are key structural features in many biologically and industrially significant molecules.

The FT-IR spectrum of the synthesized compound **1**, as depicted in the Figure 3, provides crucial evidence for the successful formation of the target molecule. The spectrum shows several characteristic absorption bands that confirm the presence of functional groups associated with the amic compound.

Key observations from the FT-IR spectrum include:

1. **ν(OH) Stretching:** The appearance of a broad band around 3450 cm^{-1} corresponds to the O–H stretching vibration. This indicates the presence of a carboxylic acid group, a common feature in amic acids, which is formed due to the reaction between the sulfamethoxazole and phthalic anhydride.
2. **ν(C=O) Carboxylic Acid:** A sharp absorption band at 1739 cm^{-1} is observed, which is characteristic of the C=O stretching vibration in the carboxylic acid group. This confirms that the carboxylic acid functionality is intact in the synthesized compound.
3. **ν(C=O) Amide:** The spectrum also shows a distinct band at 1710 cm^{-1}, which can be attributed to the C=O stretching vibration in the amide group. The presence of this band is strong evidence of the successful formation of the amide bond, resulting from the nucleophilic attack of the amino group on the carbonyl group of phthalic anhydride.

These key functional groups and their corresponding vibrational frequencies provide clear confirmation of the structural integrity of the synthesized compound **1**. The successful formation of the amic compound is indicated by the appearance of the specific absorption bands for both the carboxylic acid and amide functionalities. Other minor absorption bands in the spectrum correspond to various bending and stretching vibrations associated with the sulfamethoxazole moiety and the phthalic anhydride-derived structure, further supporting the successful synthesis of the target molecule. The detailed analysis of these bands validates the synthetic pathway employed and confirms the formation of the desired amic compound **1**, which is essential for further applications, such as corrosion inhibition or pharmaceutical use.

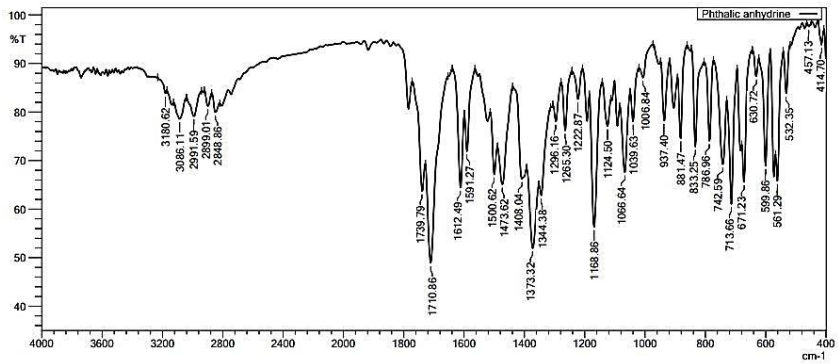

Figure 3. FT-IR spectrum of the synthesized amic compound **1** from sulfamethoxazole and phthalic anhydride.

The compound **2** was synthesized by the esterification of the previously prepared amic compound **1** with absolute ethanol, utilizing sulfuric acid as a catalyst. This reaction led to the formation of the ester functional group while retaining the amide functionality from the original compound. The successful formation of compound **2** was confirmed through FT-IR and ^{1}H-NMR spectroscopic analyses.

The FT-IR spectrum (Figure 4) of compound **2** provides clear evidence for the successful conversion of the carboxylic acid group in compound **1** to an ester group in compound **2**. This is indicated by the appearance of a strong absorption band at 1791 cm^{-1}, which corresponds to the C=O stretching vibration characteristic of ester groups. Additionally, the spectrum shows a band at 1708 cm^{-1}, which is attributed to the C=O stretching vibration of the amide group, confirming that the amide linkage remains intact following the esterification process. These key absorption bands, along with others in the spectrum, validate the chemical structure of compound **2** and confirm the successful transformation of the starting material into the desired ester. The retention of the amide band also suggests that the reaction conditions were mild enough to avoid hydrolysis or other side reactions that might have altered the amide group.

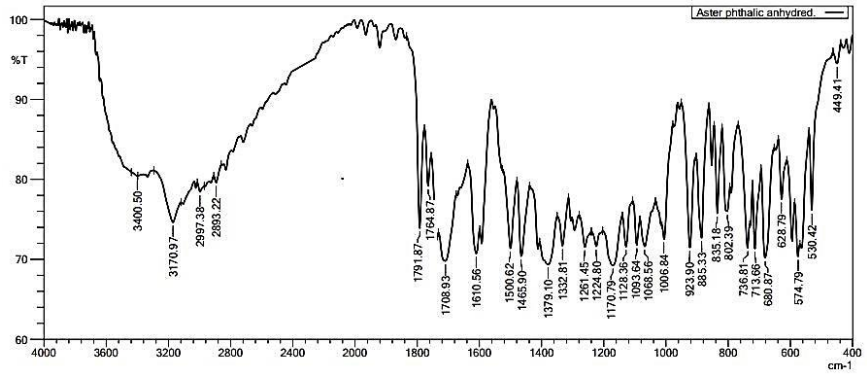

Figure 4. FT-IR spectrum of ester compound **2** derived from sulfamethoxazole amic acid.

The ^{1}H-NMR spectrum of compound **2** as in Figure 5, further supports the structural characterization. Several key signals are observed that correspond to the protons of specific functional groups in the ester compound:

- A triplet signal between δ 1.05–1.08 ppm corresponds to the protons of the methyl group in the CH_3CH_2O moiety of the ester.
- A singlet at δ 2.25 ppm is due to the protons of a methyl group (CH_3) likely attached to the isoxazole ring or another adjacent carbon atom.
- Another singlet at δ 3.73 ppm is attributed to the NH proton linked to the sulfonamide group (NH–S=O).
- A quartet at δ 3.89 ppm corresponds to the methylene protons in the CH_3CH_2O group of the ester.

- The singlet at δ 6.18 ppm is due to the proton attached to the CH=N group within the isoxazole ring.
- A multiplet between δ 7.61–7.99 ppm represents the aromatic protons of the benzene rings, indicating the presence of an aromatic system in the compound.
- A singlet at δ 8.07 ppm is associated with the NH proton of the amide group (NH–C=O).

These signals align with the expected structure of the ester compound **2** and confirm the presence of both the ester and amide functionalities within the molecule. The signals corresponding to the aromatic protons and the isoxazole ring further corroborate the successful synthesis of the compound. The signal at δ 2.50 ppm, attributed to H_2O in DMSO, is a common solvent signal and does not interfere with the interpretation of the compound's structure.

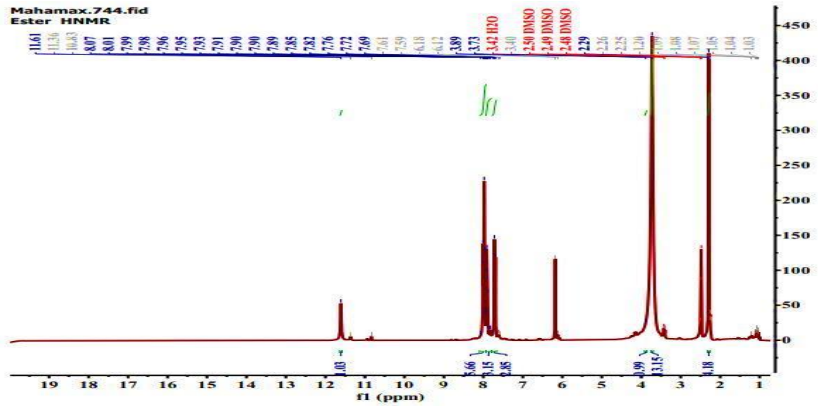

Figure 5. ^{1}H-NMR Spectrum of compound **2** derived from sulfamethoxazole amic acid.

Together, the FT-IR and ^{1}H-NMR spectra provide comprehensive evidence for the successful synthesis and structural integrity of compound **2**. The data confirm the presence of the ester and amide groups, along with the retention of other key functional groups, validating the synthetic process and the expected chemical structure.

The conversion compound **2** into its corresponding hydrazide derivative (compound **3**) was accomplished through a reaction with hydrazine hydrate. This transformation introduces a hydrazide functional group, which is of particular interest due to its potential applications in various chemical processes, including corrosion inhibition and further derivatization in organic synthesis.

The FT-IR spectrum of compound **3**, as shown in Figure 6, provides definitive evidence of the successful conversion from the ester to the hydrazide. The spectrum displays several key absorption bands that are characteristic of the newly formed hydrazide functional group.

Key observations from the FT-IR spectrum include:

1. **ν(NH_2) Asymmetric and Symmetric Stretching:** The spectrum shows absorption bands at 3425 cm^{-1} and 3356 cm^{-1}, which correspond to the asymmetric and

symmetric stretching vibrations of the NH_2 group, respectively. The presence of these bands is a clear indication of the introduction of the hydrazide group into the molecule, confirming the successful reaction with hydrazine hydrate.

2. **ν(C=O) Amide:** Although the main focus of the spectrum is on the NH_2 group, the C=O stretching vibrations characteristic of the amide functionality are also expected to be present, although they may overlap or shift due to the strong NH_2 absorptions. The exact position of this band could be correlated with the amide carbonyl stretch, typically found around 1650–1700 cm^{-1}.
3. **Additional Bands:** Other absorption bands observed in the spectrum correspond to various bending and stretching vibrations associated with the remaining parts of the molecule, such as the aromatic ring and other functional groups that remain unchanged from the parent ester compound.

The appearance of the NH_2 stretching bands at 3425 cm^{-1} and 3356 cm^{-1} is particularly significant, as it confirms the presence of the hydrazide functional group in compound **3**. These bands, in conjunction with other characteristic absorptions in the spectrum, validate the successful conversion of the ester to the hydrazide.

Overall, the FT-IR spectrum of compound **3** provides comprehensive confirmation of its structure, showcasing the presence of the key functional groups that were introduced during the chemical transformation. The data supports the successful synthesis of the hydrazide derivative, which is an important intermediate for further reactions or applications, such as in the development of corrosion inhibitors.

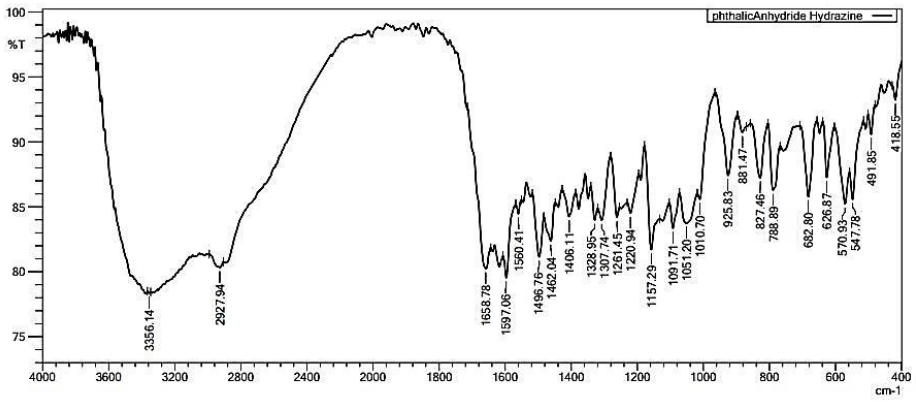

Figure 6. FT-IR spectrum of hydrazide compound **3** derived from ester compound **2**.

The conversion of the hydrazide compound **3** into pyrazole derivatives (**S1**) and (**S2**) was achieved through reactions with acetyl acetone and ethyl acetoacetate, respectively. These reactions are consistent with a nucleophilic substitution mechanism where the amino group of the hydrazide attacks the carbonyl group in the acetyl acetone or ethyl acetoacetate, followed by the elimination of ethanol, leading to the formation of the pyrazole ring. The resulting pyrazole compounds have been characterized by FT-IR spectroscopy, and the spectra provide clear evidence of the successful formation of the target compounds.

*FT-IR analysis of compound (**S1**):*

In the FT-IR spectrum as in Figure 7, of pyrazole compound (**S1**), the characteristic absorption bands for the NH_2 group, previously observed in the hydrazide (compound **3**), are no longer present. This indicates that the NH_2 group has been transformed, consistent with the formation of the pyrazole ring.

The spectrum reveals new absorption bands that are characteristic of the pyrazole structure:

- The disappearance of the NH_2 symmetric and asymmetric stretching vibrations supports the successful cyclization and formation of the pyrazole ring.
- The presence of a new absorption band around 1590 cm^{-1}, corresponding to the C=N stretching vibration, confirms the formation of the pyrazole ring structure. This C=N bond is a key feature of the pyrazole ring, indicating the successful synthesis of compound (**S1**).

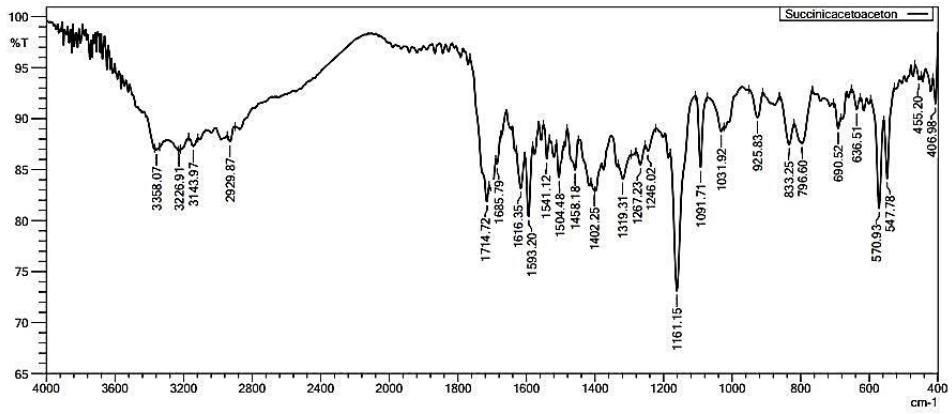

Figure 7. FT-IR spectrum of pyrazole compound (**S1**) derived from reaction of hydrazide with acetyl acetone**.**

*Proton-NMR data for compound (**S1**):*

The ^{1}H-NMR spectrum of compound **S1** provides detailed insights into its molecular structure through the distinct chemical shifts and coupling constants observed. Below is a breakdown and interpretation of the spectrum:

1. **Methyl Protons (CH_3) at δ 2.30–2.42 ppm (6H):**

- Two singlets are observed at δ 2.35 and 2.37 ppm, corresponding to the three protons (3H each) of two methyl groups (–CH_3) attached to different positions on the pyrazole ring.
- These singlets indicate that the methyl groups are in a similar chemical environment, contributing to their proximity in chemical shifts.

2. Methyl Proton (CH_3) at δ 2.66 ppm (3H, s):

- A singlet at δ 2.66 ppm represents another set of three protons (3H) from a methyl group, likely attached to a different part of the molecule, possibly adjacent to an electron-withdrawing group.
- The singlet confirms no splitting due to neighboring protons, indicating isolation from other proton-bearing atoms.

3. Aromatic Protons at δ 6.11–6.26 ppm (2H):

- Two singlets are observed at δ 6.16 and 6.21 ppm, representing the two aromatic protons on the pyrazole ring.
- The symmetry and proximity of these protons within the ring structure explain their chemical equivalence and nearly identical shifts.

4. Aromatic Protons at δ 7.56–7.69 ppm (2H):

- The signals in this region correspond to aromatic protons on the phenyl ring attached to the sulfonamide group.
- The presence of a triplet of doublets (td) at δ 7.62 and 7.63 ppm, with coupling constants (J = 7.8, 1.3 Hz and J = 7.7, 1.3 Hz), indicates vicinal coupling between these protons, suggesting they are positioned ortho and meta to other protons on the aromatic ring.

5. Aromatic Protons at δ 7.77–8.07 ppm (4H):

- A series of complex signals (ddd) are observed in this region, indicating three coupling interactions between these aromatic protons and adjacent protons.
- The doublet of doublets of doublets (ddd) at δ 7.83, 7.95, and 8.00 ppm with coupling constants (J = 7.8, 1.3, 0.5 Hz, J = 7.9, 1.5, 0.4 Hz, and J = 7.8, 1.3, 0.5 Hz) suggest that these protons are part of an aromatic system experiencing multiple interactions with adjacent protons, likely part of a disubstituted phenyl ring.

6. Aromatic Protons at δ 8.19 ppm (2H, ddd):

- The signal at δ 8.19 ppm is a doublet of doublets of doublets (ddd) with coupling constants (J = 7.9, 1.8, 0.4 Hz), suggesting these protons are at positions with slightly different electronic environments, likely part of the aromatic ring near the sulfonamide or amide group.
- The splitting patterns reflect complex coupling interactions with nearby protons, providing insight into their relative positions.

The proton NMR data of compound **S1** is consistent with its proposed structure, featuring pyrazole and aromatic rings, as well as methyl groups attached to the pyrazole ring. The chemical shifts and coupling patterns observed are indicative of the spatial arrangement and proximity of various protons in the molecule. The appearance of singlets for methyl groups and the complex splitting patterns for the aromatic protons provide clear evidence of

the compound's structural integrity. Overall, the ^{1}H-NMR spectrum supports the successful synthesis and confirmation of compound **S1**.

*FT-IR analysis for compound (**S2**):*

Similarly, the FT-IR spectrum as in Figure 8 of pyrazole compound (**S2**) shows the absence of the NH_2 stretching bands that were present in the hydrazide precursor. The transformation into the pyrazole derivative is further confirmed by the appearance of new characteristic absorption bands:

- As with compound (**S1**), the disappearance of the NH_2 bands indicates the successful formation of the pyrazole ring.
- A strong absorption band around 1590 cm^{-1} is observed, corresponding to the C=N stretching vibration, which is characteristic of the pyrazole ring structure in compound (**S2**).

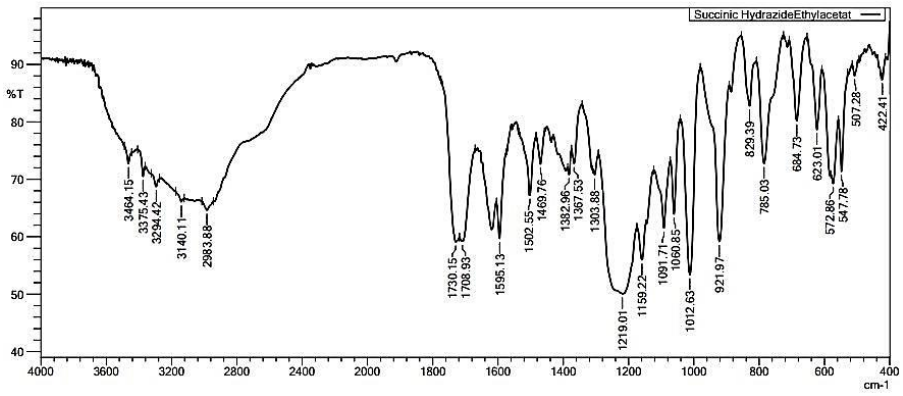

Figure 8. FT-IR spectrum of pyrazole compound (**S2**) derived from reaction of hydrazide with ethyl acetoacetate.

Both spectra demonstrate the disappearance of the NH_2 stretching vibrations (around 3356 cm^{-1}) and the emergence of new bands corresponding to the C=N bond in the pyrazole ring, thereby confirming the successful formation of the pyrazole derivatives. The consistency between the observed FT-IR spectra and the expected structures of (**S1**) and (**S2**) supports the proposed reaction mechanism and the successful synthesis of the target pyrazole compounds. These pyrazole rings play a crucial role in enhancing the electron density and potential coordination sites for metal interactions, which could be beneficial for applications such as corrosion inhibition.

*Proton-NMR data for compound (**S2**):*

The ^{1}H-NMR spectrum of compound **S2** provides valuable information about its structure and confirms the successful synthesis of the molecule. Below is a breakdown and interpretation of the key signals observed in the spectrum:

1. **Methyl Protons (CH_3) at δ 2.32–2.48 ppm (6H):**

- Two singlets are observed at δ 2.37 and 2.43 ppm, corresponding to the three protons (3H each) of two methyl groups (–CH_3) attached to different positions in the molecule.
- These singlets indicate that these methyl groups are not adjacent to any proton-bearing atoms, as there is no splitting pattern, and the chemical environments of the two methyl groups are slightly different, leading to slightly different chemical shifts.

2. **Methine Proton at δ 5.59 ppm (1H, s):**

- The singlet at δ 5.59 ppm corresponds to a single methine proton (CH) in the pyrazole ring, likely adjacent to the nitrogen atom.
- The singlet nature of this signal indicates that there are no protons directly adjacent to this methine proton, confirming its isolated position in the molecule.

3. **Aromatic Proton at δ 6.21 ppm (1H, s):**

- Another singlet at δ 6.21 ppm corresponds to an aromatic proton, likely located on the pyrazole ring. This proton is isolated in terms of coupling interactions, as evidenced by the lack of splitting, suggesting it is symmetrically positioned.

4. **Aromatic Protons at δ 7.56–7.69 ppm (2H):**

- Two protons on the aromatic ring are represented by triplet of doublets (td) at δ 7.63 ppm with coupling constants (J = 7.8, 1.3 Hz), indicating vicinal coupling. These protons are likely positioned ortho and meta to other protons on the phenyl ring, leading to the observed splitting patterns.
- The symmetrical nature of these signals suggests these protons are equivalent in their chemical environment, possibly located on the same aromatic ring near the sulfonamide group.

5. **Aromatic Protons at δ 7.77–8.02 ppm (4H):**

- In this region, we observe complex multiplet patterns (ddd) at δ 7.83, 7.88, and 7.95 ppm, with coupling constants (J = 7.8, 1.3, 0.5 Hz, J = 7.9, 1.5, 0.4 Hz, *etc.*). These signals correspond to aromatic protons in a complex coupling environment, likely on a substituted phenyl ring.
- The presence of doublet of doublets of doublets (ddd) indicates that these protons are influenced by three different neighboring protons, contributing to the complexity of the splitting pattern.

6. **Aromatic Protons at δ 8.19 ppm (2H, ddd):**

- The signal at δ 8.19 ppm is a doublet of doublets of doublets (ddd) with coupling constants (J = 7.9, 1.8, 0.4 Hz). These protons are likely positioned on the aromatic ring, with interactions from neighboring protons.

- The complexity of this signal suggests these protons are near both electron-withdrawing and electron-donating groups, which influence their chemical environment and contribute to the observed coupling.

The ^{1}H-NMR spectrum of compound **S2** shows a clear and detailed profile of the different proton environments present in the molecule. The singlet signals for the methyl and methine protons indicate isolated positions in the molecular structure, while the complex splitting patterns for the aromatic protons suggest multiple coupling interactions.

The presence of the pyrazole ring and the aromatic systems is confirmed by the chemical shifts and coupling patterns, which are consistent with the expected structure of compound **S2**. The signals observed in the aromatic region reflect the influence of substituents on the phenyl ring and the proximity of different functional groups, contributing to the distinct chemical shifts and coupling patterns observed in the NMR spectrum. Overall, the data provide strong evidence for the structure and integrity of the synthesized compound **S2**.

3.2. Anti-corrosion activity

Anti-corrosion activity: comprehensive discussion

The anti-corrosion activities of the synthesized pyrazole derivatives (**S1**) and (**S2**) were evaluated using electrochemical methods in a 1 M HCl solution. The polarization curves as in Figure 9 and associated data provide a comprehensive understanding of the inhibition efficiency (*IE*%) and the overall effectiveness of these compounds in preventing the corrosion of steel.

Polarization curves analysis

Table 1 provided highlights key parameters that quantify the corrosion inhibition performance of (**S1**) and (**S2**). For instance:

- **Corrosion Potential (E_{corr}):** Both (**S1**) and (**S2**) shift the E_{corr} to more negative values compared to the blank, indicating that these compounds act as mixed-type inhibitors, influencing both anodic and cathodic processes.
- **Corrosion Current Density (i_{corr}):** A significant reduction in i_{corr} is observed for both (**S1**) and (**S2**) compared to the blank, confirming their effectiveness in reducing the corrosion rate. Specifically, (**S2**) shows a slightly lower i_{corr} than (**S1**), suggesting better inhibition performance.
- **Polarization Resistance (Resis):** The increased polarization resistance in the presence of (**S1**) and (**S2**) compared to the blank further confirms the formation of a protective film on the metal surface, which impedes the corrosion process.
- **Anodic and Cathodic Tafel Constants (β):** The changes in Tafel constants suggest that both compounds alter the kinetics of the corrosion reactions, contributing to their overall inhibition effectiveness.

- **Corrosion Rate:** The substantial reduction in corrosion rate in the presence of (**S1**) and (**S2**) underscores the practical significance of these compounds as corrosion inhibitors.
- **Inhibition Efficiency (*IE*%):** The calculated inhibition efficiencies for (**S1**) (91%) and (**S2**) (96%) demonstrate that both compounds provide excellent protection against corrosion, with (**S2**) being slightly more effective.

Table 1. Corrosion inhibition for preparation compounds (**S1**, **S2**).

Comp	E_{corr}, V	i_{corr}, μA/cm^2	i_{corr}/r, A/cm^2	Resis., Ω·cm^2	Anodic β, V/dec	Cathodic β, V/dec	Corr. rate, mm/year	*IE*%
Blank	–0.396	248.4	$4.968 \cdot 10^{-4}$	85.01	0.121	0.081	2.438	–
S1	–0.546	22.13	$4.425 \cdot 10^{-5}$	2786	0.221	0.398	0.217	91
S2	–0.567	10.53	$2.106 \cdot 10^{-5}$	6725	0.285	0.382	0.103	96

i_{corr}/r refers to the corrosion current density normalized by the surface area of the electrode.

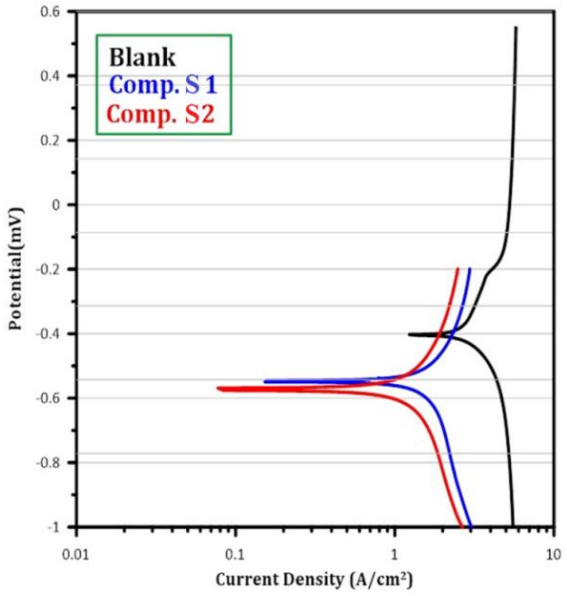

Figure 9. The combined polarization curves for the blank, (**S1**), and (**S2**) provide a direct comparison of the inhibition performance of both compounds. Both (**S1**) and (**S2**) demonstrate superior corrosion inhibition compared to the blank, with (**S2**) showing slightly better performance, as indicated by the lower i_{corr} value. The presence of the pyrazole ring in both compounds enhances their ability to adsorb onto the metal surface, thereby increasing their inhibition efficiency.

The electrochemical analysis reveals that both pyrazole derivatives (**S1**) and (**S2**) exhibit high anti-corrosion activity in acidic media, with (**S2**) showing marginally superior performance. The pyrazole ring in these compounds plays a crucial role in enhancing their adsorption onto the metal surface, thereby forming an effective protective barrier that

reduces corrosion [29]. The combined data from the polarization curves and the quantitative parameters provide strong evidence for the effectiveness of these synthesized inhibitors in preventing metal corrosion in harsh environments. This makes them promising candidates for industrial applications where corrosion resistance is critical.

3.3. Suggested mechanisms of corrosion inhibition

Figure 10 illustrates the proposed mechanisms by which the synthesized pyrazole derivatives (**S1**) and (**S2**) inhibit corrosion on metal surfaces. The interaction between the inhibitor molecules and the metal surface is crucial for understanding their anti-corrosion efficiency. Both (**S1**) and (**S2**) possess functional groups that enable them to strongly adsorb onto the metal surface, forming a protective layer that prevents corrosive species from reaching the metal substrate [30].

1. Adsorption and protective layer formation:

- **(S1) Mechanism:**
  - The molecule (**S1**) interacts with the metal surface primarily through the lone pairs of electrons on the nitrogen atoms in the pyrazole ring, the oxygen atoms in the carbonyl groups, and the sulfur atom in the sulfonamide group.
  - The blue dashed lines in the figure indicate the formation of coordinate bonds between the nitrogen and oxygen atoms of (**S1**) and the metal atoms on the surface. This interaction is likely due to the donation of electron density from the nitrogen and oxygen atoms to the metal, leading to strong adsorption.
  - The red dashed lines represent hydrogen bonding interactions between the NH groups and the metal surface. These interactions further stabilize the adsorption of (**S1**) on the metal surface, contributing to the formation of a dense and protective film that inhibits the ingress of corrosive species like chloride ions.
- **(S2) Mechanism:**
  - Similarly, (**S2**) adsorbs onto the metal surface through multiple coordination points. The nitrogen atoms in the pyrazole ring, the oxygen atoms in the carbonyl groups, and the sulfur atom in the sulfonamide group all participate in the adsorption process, as indicated by the blue dashed lines.
  - (**S2**) also features additional coordination through its NH groups, similar to (**S1**), which is indicated by the red dashed lines. The structure of (**S2**), with its additional functional groups, may provide more extensive coverage on the metal surface, potentially explaining the slightly higher inhibition efficiency observed for (**S2**) compared to (**S1**).
  - The structural differences between (**S1**) and (**S2**), particularly in the positioning and availability of coordination sites, may influence the density and uniformity of the protective film formed on the metal surface, contributing to the slight differences in their corrosion inhibition performance.

2. Role of functional groups

- Both (**S1**) and (**S2**) contain a pyrazole ring, which is known for its ability to form stable complexes with metal ions. The presence of multiple nitrogen atoms in the pyrazole ring enhances the adsorption through nitrogen-metal coordination, which is a critical factor in forming a protective barrier.
- The sulfonamide group in both compounds contains a sulfur atom, which has a high affinity for metal surfaces, particularly in acidic environments. This affinity contributes to the overall stability of the adsorbed layer [31].
- The presence of carbonyl groups (C=O) in the amide linkage and ester moiety provides additional coordination points that strengthen the adsorption of the inhibitor molecules on the metal surface.

3. Inhibition efficiency

- The comprehensive adsorption of these molecules through multiple interaction sites results in the formation of a compact and uniform protective film. This film acts as a physical barrier, reducing the accessibility of aggressive ions, such as chloride ions, to the metal surface, thereby decreasing the corrosion rate.
- The slight differences in inhibition efficiency between (**S1**) and (**S2**) can be attributed to the differences in their molecular structures, which may affect the extent and strength of adsorption. (**S2**), with its additional functional groups, may form a more extensive and possibly more uniform protective layer, leading to better corrosion inhibition.

4. Proposed mechanism summary

- The adsorption of (**S1**) and (**S2**) onto the metal surface involves a combination of coordinate bonds and hydrogen bonding interactions. The nitrogen atoms of the pyrazole rings and the oxygen atoms of the carbonyl groups serve as key sites for interaction with the metal surface.
- The resulting protective layer effectively isolates the metal from the corrosive environment, reducing the overall corrosion rate. The high inhibition efficiency observed for both (**S1**) and (**S2**) is a direct consequence of these strong and extensive adsorption interactions.

In conclusion, the proposed mechanisms illustrated in Figure 10 provide a clear understanding of how the pyrazole derivatives (**S1**) and (**S2**) act as effective corrosion inhibitors. The multiple interaction points within these molecules allow for strong adsorption onto the metal surface, forming a protective barrier that significantly reduces corrosion. The slight structural differences between (**S1**) and (**S2**) account for the observed variations in their corrosion inhibition efficiencies, with (**S2**) potentially offering more extensive surface coverage and, consequently, better protection.

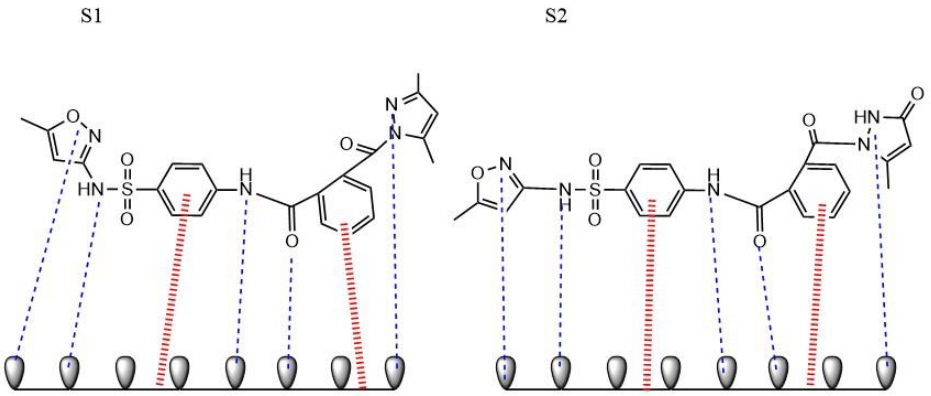

Figure 10. Suggested inhibition mechanism.

Conclusion

This research has successfully synthesized and characterized novel pyrazole-based derivatives, specifically compounds (**S1**) and (**S2**), and evaluated their efficacy as corrosion inhibitors in acidic environments. The structural analysis, confirmed by FT-IR and ^{1}H-NMR spectroscopy, validated the formation of the desired compounds. The electrochemical studies, including potentiodynamic polarization, demonstrated that both (**S1**) and (**S2**) possess significant corrosion inhibition properties, with (**S2**) exhibiting slightly higher inhibition efficiency. The anti-corrosion mechanisms of (**S1**) and (**S2**) were elucidated through the analysis of their interactions with the metal surface. Both compounds form protective layers on the metal surface through adsorption, primarily driven by the pyrazole ring's nitrogen atoms and additional coordination sites provided by functional groups such as carbonyl and sulfonamide groups. These interactions create a robust barrier that effectively reduces the metal's exposure to corrosive agents, thus significantly decreasing the corrosion rate. The findings of this study indicate that the synthesized pyrazole derivatives are highly effective as corrosion inhibitors, making them promising candidates for industrial applications where metal corrosion is a critical concern. The slight difference in performance between (**S1**) and (**S2**) suggests that further modifications of these compounds could optimize their protective abilities, opening avenues for the development of even more efficient corrosion inhibitors. Future studies could explore the long-term stability and environmental impact of these inhibitors, as well as their effectiveness in different corrosive environments, to fully realize their potential in corrosion protection strategies.

References

1. A.V. Karaulova, A.Yu. Luchkin, O.A. Goncharova and N.N. Andreev, Features of steel protection by chamber inhibitors based on a mixture of octadecylamine and benzotriazole, *Int. J. Corros. Scale Inhib.*, 2024, **13**, no. 2, 671–682. doi: 10.17675/2305-6894-2024-13-2-2

2. V.E. Kasatkin, L.P. Kornienko, A.I. Shcherbakov, I.V. Kasatkina, I.G. Korosteleva and V.N. Dorofeeva, Investigation of nickel electrochemical impedance spectra under conditions of anodic polarization in hydroxide solutions with chloride ion additives, *Int. J. Corros. Scale Inhib*., 2024, **13**, no. 2, 683–707. doi: 10.17675/2305-6894-2024-13-2-3
3. M.F. Atia, A.M. Hamzah, M.E. Eissa, A. El-Hossiany and A.S. Fouda, Haloxylon salicornicum extract as an eco-friendly corrosion inhibitor for carbon steel in HCl solution, *Int. J. Corros. Scale Inhib*., 2024, **13**, no. 2, 750–774. doi: 10.17675/2305-6894-2024-13-2-6
4. N. Muneam, F.F. Sayyid, M.H.H. Al-Kaabi and A.A. Alamiery, Environmentally friendly synthesis and characterization of copper nanoparticles using amino acids as capping agents: enhanced corrosion resistance and morphological control, *Int. J. Corros. Scale Inhib*., 2024, **13**, no. 1, 288–310. doi: 10.17675/2305-6894-2024-13-1-14
5. E.A. Zheludkova, A.A. Abrashov, V.A. Sukhorukova, N.S. Grigoryan, A.V. Sundukova, O.Yu. Grafov and T.A. Vagramyan, Passivation of galvanized steel in a solution based on cerium and lanthanum compounds, *Int. J. Corros. Scale Inhib*., 2024, **13**, no. 2, 775–789. doi: 10.17675/2305-6894-2024-13-2-7
6. S.M. Reshetnikov, A.V. Tyukalov, F.Z. Gil'mutdinov, E.B. Kharanzhevskii, A.R. Gazizyanova, A.S. Shirobokova and A.I. Chukavin, Enhancing the corrosion resistance of oxide-ceramic composites by the cyclic anodic polarization technique, *Int. J. Corros. Scale Inhib*., 2024, **13**, no. 2, 812–822. doi: 10.17675/2305-6894-2024-13-2-9
7. A.M. Mustafa, F.F. Sayyid, N. Betti, L.M. Shaker, M.M. Hanoon, A.A. Alamiery, A.A.H. Kadhum and M.S. Takriff, Inhibition of low carbon steel corrosion in hydrochloric acid environment by 1-amino-2-mercapto-5-(4-(pyrrol-1-yl)phenyl)-1,3,4-triazole, *S. Afr. J. Chem. Eng*., 2022, **39**, 42–51. doi: 10.1016/j.sajce.2021.11.009
8. Sheetal, S. Sengupt, M. Singh, S. Thakur, B. Pani, P. Banerjee, S. Kaya and A. Singh, An insight about the interaction of Aryl Benzothiazoles with low carbon steel surface in aqueous HCl solution, *J. Mol. Liq*., 2022, **354**, 118890. doi: 10.1016/j.molliq.2022.118890
9. A.M. Resen, M.M. Hanoon, W.K. Alani, A. Kadhim, A.A. Mohammed, T.S. Gaaz, A.A.H. Kadhum, A.A. Al-Amiery and M.S. Takriff, Exploration of 8-piperazine-1-ylmethylumbelliferone for application as a corrosion inhibitor for low carbon steel in hydrochloric acid solution, *Int. J. Corros. Scale Inhib*, 2021, **10**, no. 1, 368–387. doi: 10.17675/2305-6894-2021-10-1-21
10. D.K. Verma, M. Kazi, M.S. Alqahtani, R. Syed, E. Berdimurodov, S. Kaya, R. Salim, A. Asatkar and R. Haldhar, N–hydroxybenzothioamide derivatives as green and efficient corrosion inhibitors for low carbon steel: Experimental, DFT and MC simulation approach, *J. Mol. Struct*., 2021, **1241**, 130648. doi: 10.1016/j.molstruc.2021.130648
11. R. Haldhar, D. Prasad, I. Bahadur, O. Dagdag and A. Berisha, Evaluation of *Gloriosa superba* seeds extract as corrosion inhibition for low carbon steel in sulfuric acidic medium: A combined experimental and computational studies, *J. Mol. Liq*., 2021, **323**, 114958. doi: 10.1016/j.molliq.2020.114958

12. A.M. Mustafa, F.F. Sayyid, N. Betti, M.M. Hanoon, A. Al-Amiery, A.A.H. Kadhum and M.S. Takriff, Inhibition Evaluation of 5-(4-(1*H*-pyrrol-1-yl)phenyl)-2-mercapto-1,3,4-oxadiazole for the Corrosion of Low carbon Steel in an Acid environment: Thermodynamic and DFT Aspects, *Tribologia*, 2021, **38**, no. 3–4, 39–47. doi: 10.30678/fjt.105330
13. A.M. Resen, M.M. Hanoon, R.D. Salim, A.A. Al-Amiery, L.M. Shaker and A.A.H. Kadhum, Gravimetrical, theoretical, and surface morphological investigations of corrosion inhibition effect of 4-(benzoimidazole-2-yl)pyridine on low carbon steel in hydrochloric acid, *Koroze Ochr. Mater*., 2020, **64**, no. 4, 122–130. doi: 10.2478/kom-2020-0018
14. P. Kumari, G. Anusha, J. Mishma, R. Sinha, A. Suvarna and S. Gaonkar, New benzisoxazole derivative: A potential corrosion inhibitor for low carbon steel in 0.5 M hydrochloric acid medium-insights from electrochemical and density functional theory studies, *Heliyon*, 2023, **9**, e21014. doi: 10.1016/j.heliyon.2023.e21014
15. B.S. Mahdi, M.K. Abbass, M.K. Mohsin, W.K. Al-Azzawi, M.M. Hanoon, M.H.H. AlKaabi, L.M. Shaker, A.A. Al-Amiery, W.N.R.W. Isahak, A.A.H. Kadhum and M.S. Takriff, Corrosion inhibition of mild steel in hydrochloric acid environment using terephthaldehyde based on Schiff base: Gravimetric, thermodynamic, and computational studies, *Molecules*, 2022, **27**, no. 15, 4857. doi: 10.3390/molecule**S2**7154857
16. M. Rezaeivala, S. Karimi, K. Sayin and B. Tüzün, Experimental and theoretical investigation of corrosion inhibition effect of two piperazine-based ligands on carbon steel in acidic media, *Colloids Surf. A*, 2022, **641**, 128538. doi: 10.1016/j.colsurfa.2022.128538
17. H.P. Liu, N. Li, S.F. Bi, D.Y. Li and Z.L. Zou, Effect of organic additives on the corrosion resistance properties of electroless nickel deposits, *Thin Solid Films*, 2008, **516**, no. 8, 1883–1889. doi: 10.1016/j.tsf.2007.10.008
18. B.T.SH. AL-Mosawi, The use of laser ablation technique for the synthesis of titanium dioxide nanoparticles synergistic with sulfamethoxazole to prepare an anti-corrosion surface coating for mild steel and study of refraction and absorption, *Int. J. Corros. Scale Inhib*., 2020, **9**, no. 3, 1025–1036. doi: 10.17675/2305-6894-2020-9-3-15
19. T. Ramdé, S. Rossi and L. Bonou, Corrosion Inhibition Action of Sulfamethoxazole for Brass in Acidic Media, *Int. J. Electrochem. Sci*., 2016, **11**, no. 8, 6819–6829. doi: 10.20964/2016.08.39
20. F.M. Ibrahim, R.A. Hammza and D.H. Fadhil, Synthesis and characterization of Trimethoprim metal complexes used as corrosion inhibitors for carbon steel in acid media, *Int. J. Corros. Scale Inhib*., 2019, **8**, no. 3, 733–742. doi: 10.17675/2305-6894-2019-8-3-20

21. F. Zulkifli, S. Khairina, M.S.M. Ghazali, A.A. Al-Amiery, N. Ismail, V.O. Izionworu, M.J. Suriani and W.B.W. Nik, Application of electrochemical impedance spectroscopy technology to evaluate passivation performance of film forming and adsorption types corrosion inhibitors, *Int. J. Corros. Scale Inhib*., 2022, **11**, no. 3, 1303–1318. doi: 10.17675/2305-6894-2022-11-3-23
22. Ya.G. Avdeev, E.N. Yurasova, K.L. Anfilov and T.A. Vagramyan, Protection of low-carbon steel in solutions of mineral acids by nitrogen-containing pharmaceutical agents of triphenylmethane series, *Int. J. Corros. Scale Inhib*., 2018, **7**, no. 1, 87–101. doi: 10.17675/2305-6894-2018-7-1-8
23. B.F. Hamzah, I. Taha, Z.M. Najm, M.D. Husseini and N.S.K. Al-Khafaji, Synthesis, Characterization, and Antibacterial Activity of Some New Oxazepine Derivatives, *J. Med. Chem. Sci*., 2023, **6**, no. 6, 1239–1245.
24. A. Al-Azzawi and A. Hassan, Synthesis and Antimicrobial Activity of New Succinimides Bearing Different Heterocyclics, *Int. J. Res. Pharm. Chem*., 2014, **4**, no. 4, 755–762.
25. ASTM G1-03, *Standard Practice for Preparing, Cleaning, and Evaluating Corrosion Test*, 2011.
26. A.S. Fouda, M.A. Ismail, A.S. Abousalem and G.Y. Elewady, Experimental and theoretical studies on corrosion inhibition of 4-amidinophenyl-2,2′-bifuran and its analogues in acidic media, *RSC Adv*., 2017, **7**, 46414–46430. doi: 10.1039/C7RA08092A
27. Z. El kiri, K. Dakhsi, N. Dkhireche, A. Hmada, H. Bidi, F. Benhiba, M. Galai, R. Hsissou, A. Habsaoui and M. Ebn Touhami, Correlation between experimental and theoretical approaches in the performance of new epoxy resin as an effective corrosion inhibitor for mild steel in acid pickling bath, *Int. J. Corros. Scale Inhib*., 2024, **13**, no. 2, 823–852. doi: 10.17675/2305-6894-2024-13-2-10
28. R. Zhang, H. Yang, Y. Sun, W. Song, X. Zhu, N. Wang, Y. Wang, Y.C. Pan and Z. Zhang, Competitive Adsorption of 4-Methyl-4*H*-1,2,4-triazole-3-thiol and Na Salt of Phytic Acid on a Silver Surface: Raman Spectral and Electrochemical Observations, *J. Phys. Chem. C*, 2009, **113**, no. 22, 9748–9754. doi: 10.1021/jp900329s
29. Sheetal, A. Singh, M. Singh, S. Thakur, B. Pani and S. Kaya, Advancement of corrosion inhibitor system through N-heterocyclic compounds: a review, *Corrosion Engineering, Science and Technology*, 2023, **58**, no. 1, 73–101.
30. J.C. Valle-Quitana, G.F. Dominguez-Patiño and J.G. Gonzalez-Rodriguez, Corrosion Inhibition of Carbon Steel in 0.5 M H_2SO_4 by Phthalocyanine blue, *Int. Scholarly Res. Not*., 2014, **2014**, no. 1, 945645. doi: 10.1155/2014/945645
31. P. Zhao, Q. Liang and Y. Li, Electrochemical, SEM/EDS and quantum chemical study of phthalocyanines as corrosion inhibitors for low carbon steel in 1 mol/L HCl, *Appl. Surf. Sci*., 2005, **252**, no. 5, 1596–1607. doi: 10.1016/j.apsusc.2005.02.121

♦ ♦ ♦